LIMNOLOGY and OCEANOGRAPHY: METHODS

ASLO

Limnol. Oceanogr.: Methods 21, 2023, 169–177

doi: 10.1002/lom3.10537

Image analysis and benthic ecology: Proceedings to analyze in situ long-term image series

Romero-Ramirez Alicia,[1]* **Morales Luna Hadrys Laura**,[2] **Kuklinski Piotr**,[2] **Chelchowski Maciej**,[2] **Balazy Piotr**[2]

[1]University of Bordeaux, EPOC-UMR 5805, Arcachon, Aquitaine, France
[2]Polska Akademia Nauk Instytut Oceanologii, Sopot, Poland

Abstract

Long time series of underwater images have become a tool widely used within the benthic ecology research community. The development of new acquisition systems with bigger storing capacities lead researchers and scientists to deploy them for longer periods resulting in large amounts of data. This paper focuses on the first steps of analyzing large numbers of underwater images, which involves assessing the amount of valid data while assuming no technical problems. The question here addressed is how many of the in situ images can reliably be really used for benthic ecology purposes. To answer this question, we propose a method to eliminate nonvalid images and use it with four different sets of time-lapsed images acquired for long periods ranging from 73 to 371 ds in a row. The results show that elimination of between 8% and 22% of the images is possible depending on the data set. The main advantage of the method is easing and accelerating automation of subsequent analysis.

The importance of coastal and marine observations to acquire knowledge and the need for an increase of marine biological observation is a topical subject for researchers, marine policies decision makers and conservation managers (Bax et al. 2019; Estes et al. 2021). Biological ocean observations can be any data collected in a systematic and regular way on living ocean inhabitants (She et al. 2019). One example of this data could be time-lapse images and video recordings like at the cabled ocean observatory, NEPTUNE (Barnes et al. 2007, 2011) or the HAUSGARTEN (Soltwedel et al. 2005).

The use of time-lapse images (or video recordings) as a tool to study marine biology and ecology is commonly done within the benthic ecology research community (Smith et al. 1993; Kaufmann and Smith 1997; Maire et al. 2006; Bernard et al. 2016; Balazy et al. 2021). Time-lapse images can provide novel data that could not be acquired otherwise on the seabed (Bett 2003) and can capture events that are rare, unknown or unpredictable. Long-term deployments are used to study slow-moving biological and geological phenomena that are otherwise unnoticeable in the short term as well as in the deep or remote areas where direct human access is limited (Smith et al. 1993; Kaufmann and Smith 1997; Bett 2003; Eleftheriou 2013; Smith and Rumohr 2013).

Information extracted from a time-lapse camera deployment for benthic surveys can be spatial or temporal in nature. Mobile platforms like remotely operated vehicles and autonomous underwater vehicles are frequently used for spatial information such as the study of benthic biodiversity, faunal composition and habitat mapping (Spencer et al. 2005; Cuvelier et al. 2012; Williams et al. 2012; Pizarro et al. 2013; Duffy et al. 2014; Mallet and Pelletier 2014; Gauci et al. 2020; Jac et al. 2021). Static platforms, for example benthic landers, are used to obtain temporal information such as the characterization and quantification of biological behaviors and activities (Lampitt 1990; Maire et al. 2007*a*; Matabos et al. 2011, 2015; Schories et al. 2020) and the bioturbation rates of benthic fauna (Bett and Rice 1993; Solan et al. 2004; Maire et al. 2006, 2007*b*; Vardaro et al. 2009; Bernard et al. 2012).

Among the difficulties in long-time in situ submerged machines and systems, biofouling and corrosion are problems that can be particularly troublesome for underwater cameras. Biofouling disturbs camera lenses and strobes needed for complete visibility of the system. Systems deployed for long periods require periodic cleanings in the field (Baschek et al. 2017) or expensive mechanical antifouling tools (Balazy et al. 2018) as most of the available antifouling coatings are not transparent and can affect the benthic organisms in the direct vicinity.

*Correspondence: alicia.romero-ramirez@u-bordeaux.fr

Author Contribution Statement: The work and effort of each of the authors has been necessary to achieve this manuscript. The conception and design of this study have been directed by the first (A.R.R.) and the last author (P.B.).

Apart from these well-known problems, there are other causes responsible for a decrease in the visibility of in situ time-lapse systems. These include the increase of water turbidity and the variability of natural light conditions (particularly in shallow waters due to storm events or freshwater discharge), the appearance of mobile megafauna and large swarms of plankton that can be light-attracted, and the presence of seaweeds and other marine debris dragged with ocean currents to list a few.

Within the context of acquiring a long series of images from the seabed by a static device, this article focuses on assessing the number of valid images for information extraction. Other than technical problems during deployment, this is the first question to address before assessing any benthic ecology issue. Manual image classification (like usable or nonusable image) is very time-consuming and often operator-dependent. Verifying the validity of images needs to be done prior to any further analysis. An automatic solution would reduce: (1) the time needed to manually sort the images out and (2) the computational resources needed since there will be fewer images to be analyzed. This paper presents a method based on the dissimilarity of the gray-level co-occurrence matrix (GLCM) to automatically classify images into usable or not usable. This study is part of our experience analyzing large data sets acquired with a time-lapse camera system monitoring the activity of benthic filter feeders in the Arctic conditions.

Materials and methods

Data acquisition

Images were taken using a diver deployed autonomous time-lapse system specially developed for ecological studies (Balazy et al. 2018). Four identical systems were deployed in four different places in the high-Arctic (Spitsbergen Island, Svalbard Archipelago, 78°N) and in the sub-Arctic (Northern Norway, 68°N) at depths of 17–20 m. The time-lapse systems were set up to acquire an image every 30 min during long periods (Table 1). Camera 3 and Camera 4 were deployed for a complete year; however, they were recovered after a period of 186 and 174 d and relaunched for 180 and 197 d, respectively. The recovery and redeployment time was between 1 and 2 days in which: (1) the battery of the camera was recharged, (2) the camera housing was cleaned and (3) the memory card was emptied.

Data processing and analysis

In order to analyze this large number of images we used AviExplore (Romero-Ramirez et al. 2016), a software developed for video analysis with benthic applications. Time-lapse series of images were converted into avi-formatted video files.

In studies of texture in images, the most prevalent technique is the GLCM (Coburn and Roberts 2004). The co-occurrence matrix is a transformation of an image based on how often a pair of pixels with specified values and spatial relationship occurs in an image (Chatterjee et al. 2022). When the co-occurrence transformation is done on the gray-scale image, the resulting matrix is called the GLCM. Different disciplines such as medicine (Aborisade et al. 2014; Aggarwal 2022) and remote sensing (Haralick 1979; Ferro and Warner 2002; Coburn and Roberts 2004; Hall-Beyer 2017*b*) use the GLCM as a technique of texture analysis.

Several features can be extracted and computed from the GLCM (Haralick et al. 1973; Hall-Beyer 2017*a*). The GLCM dissimilarity represents the heterogeneity in the image texture (Aggarwal 2022) and is commonly used as a texture feature that defines the variation of gray level pairs (pixel and its neighbor) in an image. For each image, the dissimilarity of the GLCM is computed following Eq. 1, where i and j correspond to the horizontal and vertical coordinate in the GLCM, $P_{i,j}$ is the probability value recorded for the cells i, j, and N is the number of row or columns.

$$\sum_{i,j}^{N-1} P_{i,j} \, | \, i - j \, | \tag{1}$$

The mean and the standard deviation of the dissimilarity GLCM are computed. The usable range of values is here defined by the mean ± standard deviation. Images with higher dissimilarity values than the mean plus the standard deviation and lower dissimilarity values than the mean − standard deviation were classified as nonusable images.

Table 1. Summary of the location and period of the camera deployment.

	Camera 1	Camera 2	Camera 3	Camera 4
Location	Longyearbyen	Longyearbyen	Longyearbyen	Tromso
GPS position	78°11′18.5″N	78°11′18.3″N	78°11′18.0″N	69°31′53.3″N
	15°08′41.6″E	15°08′41.4″E	15°08′41.1″E	19°03′23.2″E
Period of acquisition	02 Aug 2019–15 Oct 2019	28 Jul 2019–15 Oct 2019	28 Jul 2019–27 Jul 2020	18 Jul 2019–22 Jul 2020
Total number of days	75	80	366 (186 + 180)	371 (174 + 197)
Recover time (days)	No	No	Yes (1.5 d)	Yes (1 d)
Number of images	3524	3669	17,901	17,737
			First set: 8634	First set: 8321
			Second set: 9267	Second set: 9415

In order to proceed with a visual validation, a trained operator classified the complete set of images into valid or not valid. A valid image is here defined as an image where the human operator was able to see at least 50% of the filter feeders present in the image. We calculate the total percentage of nonusable images for each camera.

A well-classified image for the automatic method is here defined by the agreement with the visual operator, which means that the automatic and the visual classification have the same label. Thus, the performance of the proposed automatic method is measured by the accuracy. The accuracy is calculated by the number of images well classified by the automatic method divided by the total number of images.

In order to summarize the results of the four different cameras, we calculate a weighted mean percentage of images classified as: (1) nonusable with the method and (2) nonusable by the trained operator. The agreement between both classifications (accuracy) was measured as the number of images agreeing divided by total number of images.

Results

Figures 1–4 show the GLCM dissimilarity value for each of the images corresponding to camera 1, 2, 3, and 4, respectively, with examples of images. For each data set, the mean GLCM dissimilarity value is represented with a straight line whereas the standard deviation is represented with dash lines.

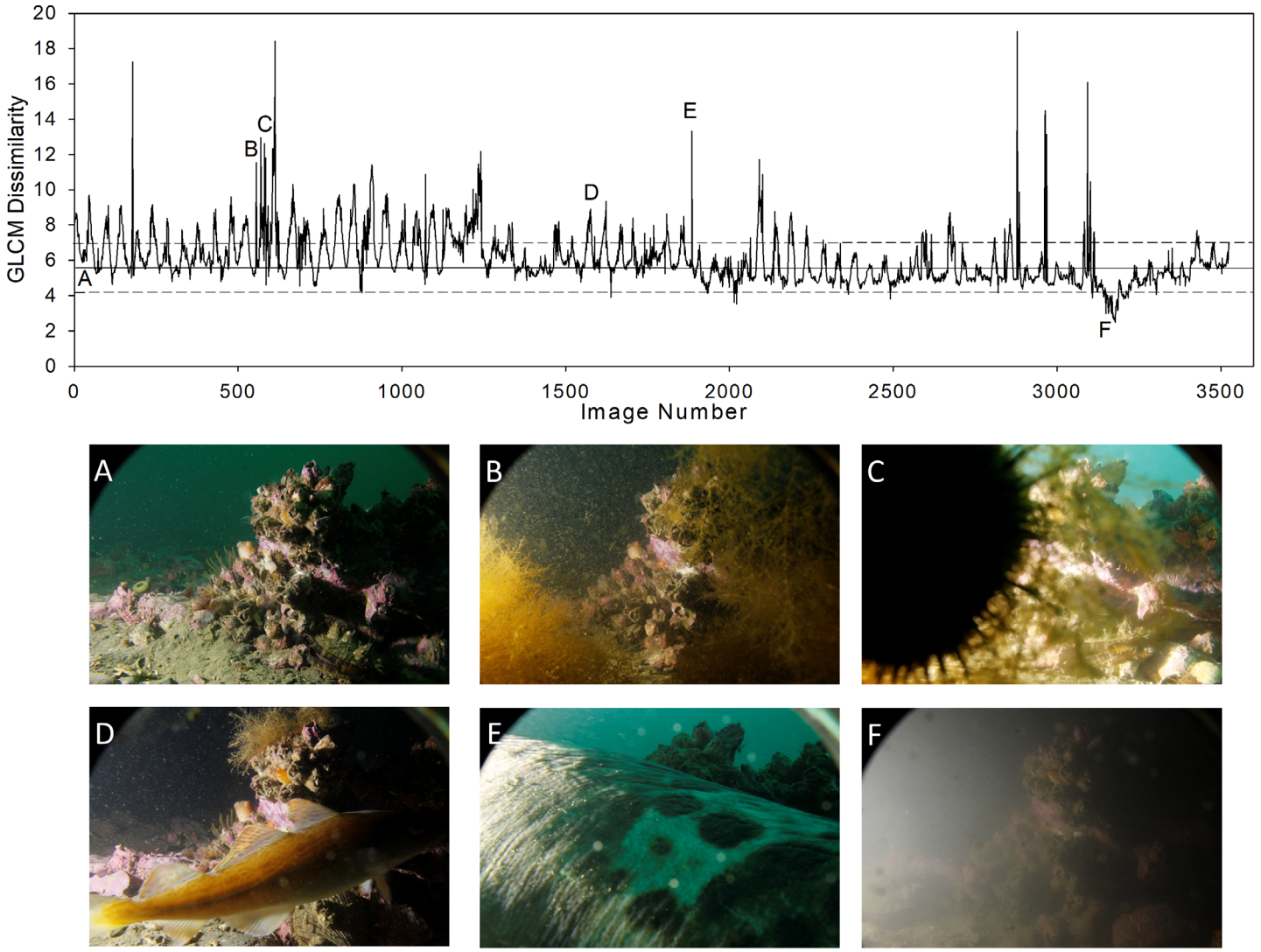

Fig. 1. Results from the GLCM values of the complete image series of camera 1 located in Longyearbyen. The continuous line represents the mean GLCM value (m), the dashed lines represent the mean ± standard deviation (s). (**A**) Image with GLCM values in the range ($m - s$, $m + s$), (**B**–**F**) images with GLCM values outside the range ($m - s$, $m + s$).

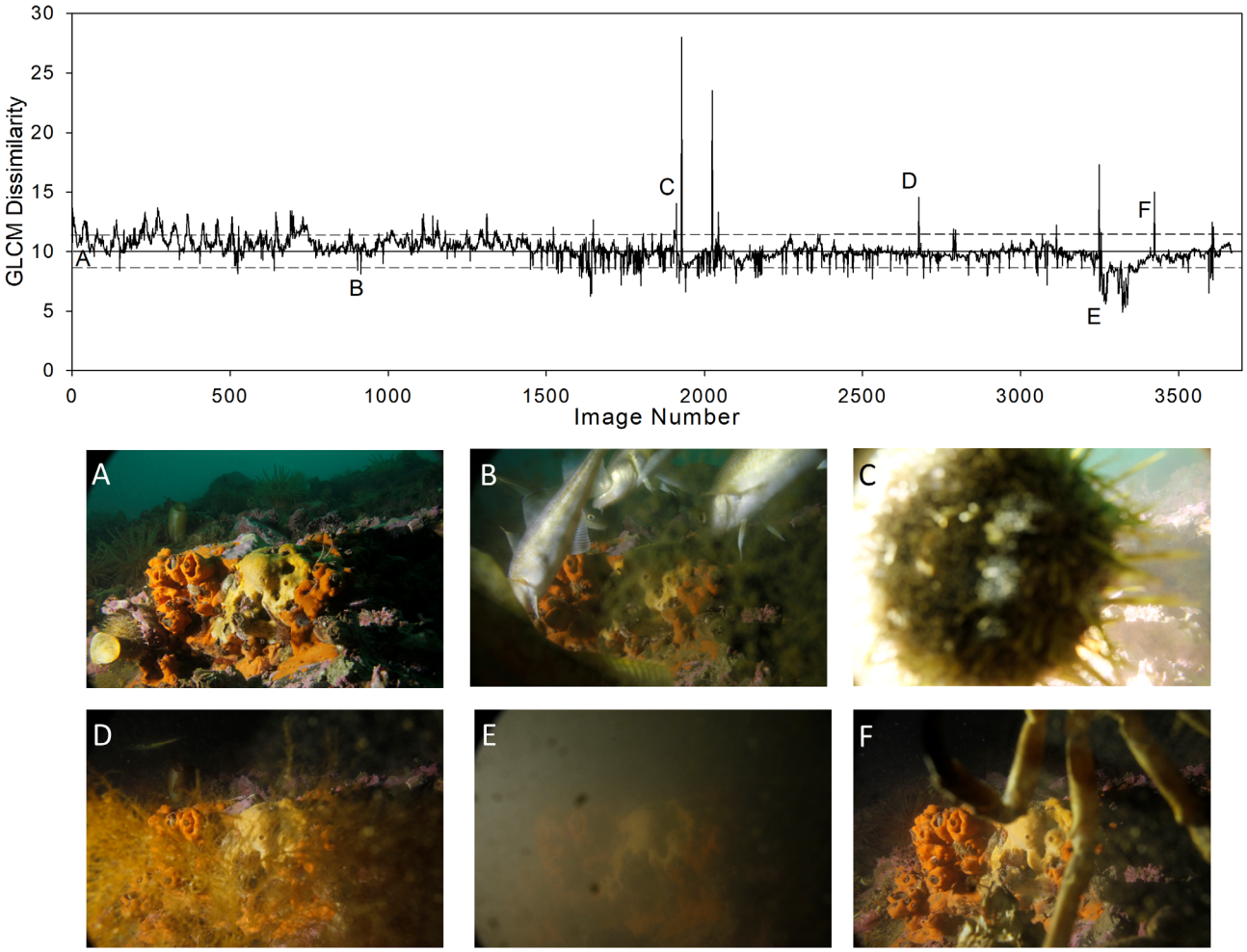

Fig. 2. Results from the GLCM values of the complete image series of camera 2 located in Longyearbyen. The continuous line represents the mean GLCM value (m), the dashed lines represent the mean ± standard deviation (s). (**A**) Image with GLCM values in the range ($m - s$, $m + s$], (**B**–**F**) images with GLCM values outside the range ($m - s$, $m + s$).

Different images A, B, C, D, E, and F are shown to illustrate the use of GLCM dissimilarity values to eliminate images. For all the figures, image A belongs to the range of usable images and allows visualizing the benthic ecological interest of the image series. It is to be noted that not all of the images with dissimilarity values beyond the usable range are not ecologically usable; this is the case in Fig. 3C where only a part of the image is hidden by the crab. In this example, this image is still labeled as usable by a trained expert.

Results of the classification can be compared with those from the visual validation in Table 2. Except for camera 4, the number of images that were visually nonusable (validation) were lower than with the method (classification); the main reason is that this method is detecting events like the appearance of fauna or algae that might (or might not) hide the filter feeders present in an image. Accuracy values varied between 82.09% and 91.91%. The weighted mean shows similar values for the classification and the validation achieving a total accuracy of 88.68%.

Discussion and conclusions

Automatic image analysis for image series

The question addressed in this paper focuses on assessing the number of valid images available for information extraction before any other further analysis. To our knowledge, this question has not specifically been studied before. However, within the development of underwater camera traps, automated classification algorithms are used to sort out images containing fish or not (Bilodeau et al. 2022), and this part of the work can be compared to the detection of usable or nonusable images in this study.

The analysis of image series from the seabed is often done manually (Chauvet et al. 2018) which is very time-consuming

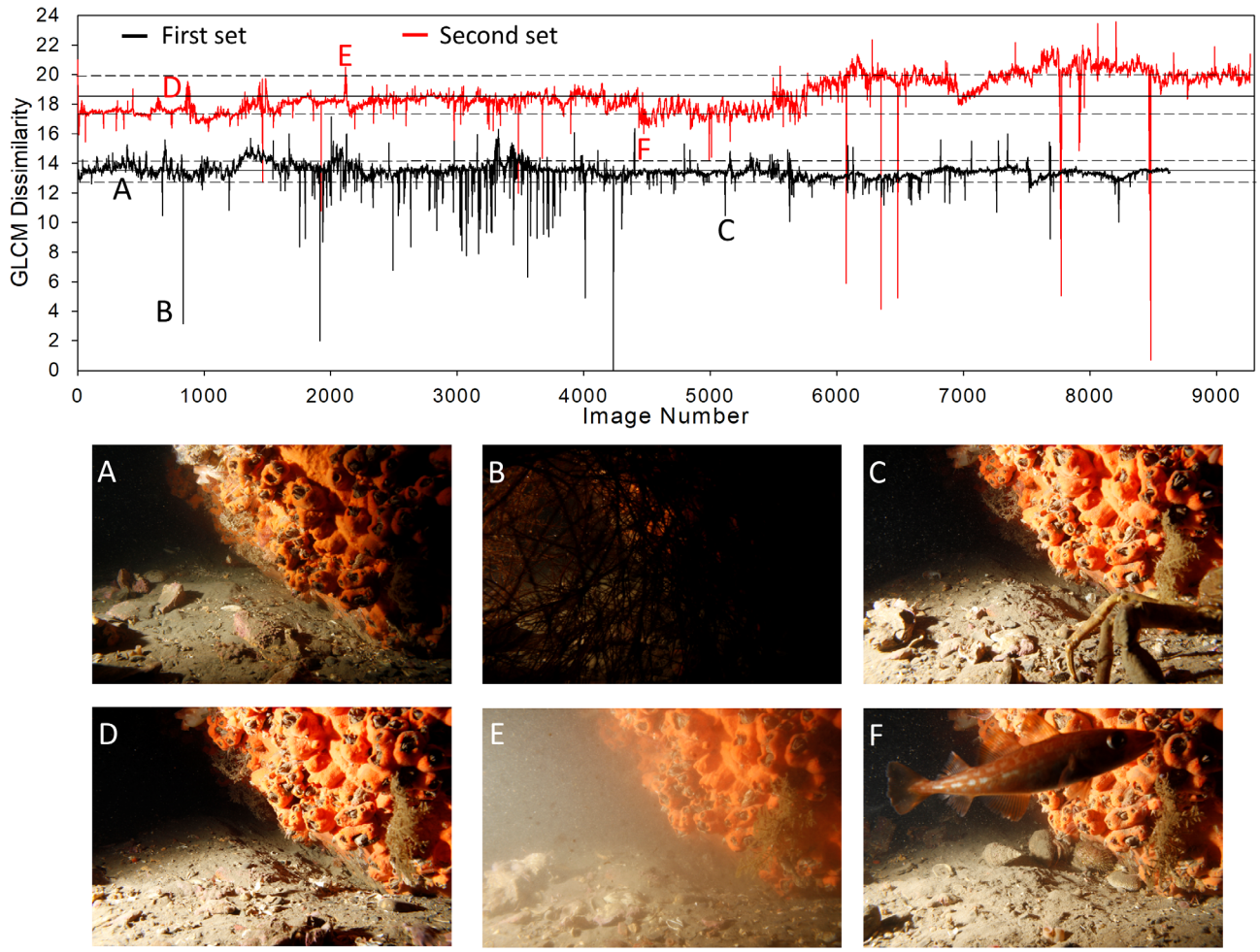

Fig. 3. Results from the GLCM values of the complete image series of camera 3 located in Longyearbyen. The continuous line represents the mean GLCM value (m), the dashed lines represent the mean ± standard deviation (s). (**A**) Image with GLCM values in the range ($m - s$, $m + s$), (**B**–**F**) images with GLCM values outside the range ($m - s$, $m + s$).

and often operator-dependent. Our method aims to clean up data sets containing information not relevant for benthic surveys. It is to be noted that there is currently a big effort from the community to use deep learning algorithms to automatically extract spatial information (Katija et al. 2022). Temporal surveys using static platforms need also to lighten the manual analysis.

When a researcher recovers his equipment that has been submerged for a long period, he always wonders if the data would be properly acquired for the intended purpose. Our experience here relates to time-lapse photography system, but the same kind of disturbances are to be expected for other types of sensors deployed for a long period. Other equipment can also be affected with similar artifacts namely the increase of water turbidity, appearance of megafauna, swarms of plankton and seaweeds. In our study, these issues represented between 3% and 31% of the data with a weighted mean of 15.62%.

Long-term series of images normally come from a deep-sea observatory with relatively stable hydrodynamic conditions (Chauvet et al. 2018, 2019). The long time series of images used for our work came from shallow waters in a polar region. Although this data set is unique; the proposed method has potential to work in very different conditions.

The method and its results

The proposed method achieved a weighted total accuracy of 88.69%. Although there is a need for an increase in accuracy, the goal here was also to propose a solution that was fast and easy to implement. The agreement between the operator and the method is related to the definition of a non-valid image. For instance, the method excludes more images than the human would do; the reason for that is linked to the size of the hidden part of an image and the selected range of values ($\bar{x} - \sigma$, $\bar{x} + \sigma$) that are classifying images as usable. For example, the image in Fig. 3C is automatically classified as nonusable because of the presence of fauna, but this image is visually classified as valid. Thus, the proposed method could also be seen as a detector of events like the appearance of macrofauna, fish or algae. If more of those events would

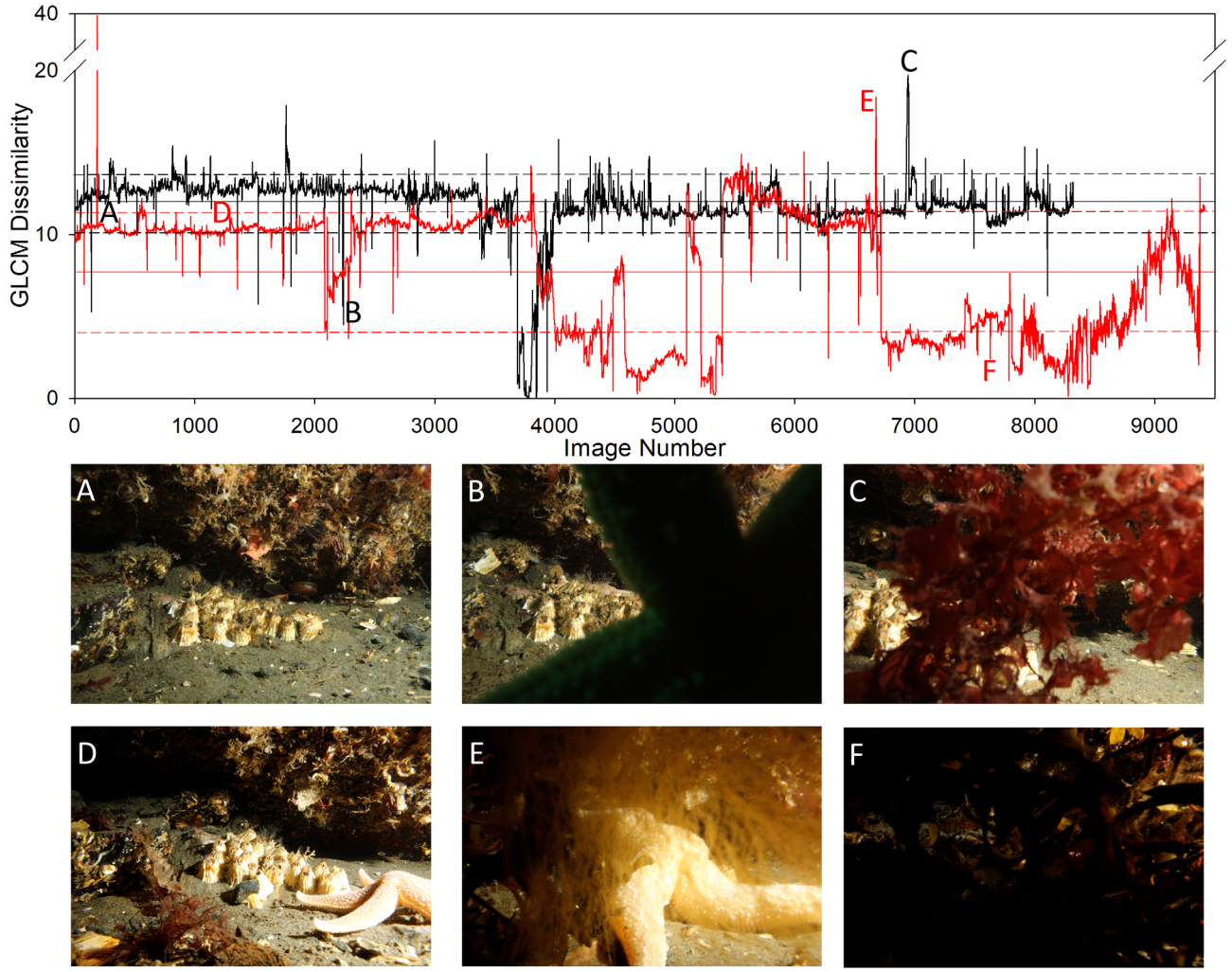

Fig. 4. Results from the GLCM values of the complete image series of camera 4 located in Tromso. The continuous line represents the mean GLCM value (m), the dashed lines represent the mean ± standard deviation (s). (**A**,**D**) Images with GLCM values in the range ($m - s$, $m + s$), (**B**,**C**,**E**,**F**) images with GLCM values outside the range ($m - s$, $m + s$).

Table 2. Results from classification and validation for the different cameras assessed.

	Camera 1	Camera 2	Camera 3	Camera 4	Overview (weighted mean)
Classification	18.32	20.55	8.23	21.94	15.79
Nonusable images (%) ($\bar{x} \pm \sigma$)					
Validation	12.85	5.51	3.03	30.99	15.62
Nonusable images (%)					
Accuracy (%)	87.23	82.09	91.91	87.09	88.68
Data 1 (when camera retrieved)			87.85	89.56	
Data 2 (when camera retrieved)			95.99	84.62	

need to be classified as usable images then an increase of the range of dissimilarity values (i.e., $[\bar{x} - 2\sigma, \bar{x} + 2\sigma]$) would be necessary; on the other hand, if more of those events would need to be classified as nonusable then the range of dissimilarity values should be decrease.

The GLCM and its associated texture features (Haralick et al. 1973) are an image analysis technique normally used in different textural image classification applications. Here, we propose to use the dissimilarity in the GLCM as a measure to classify the image. Since some of the features extracted from

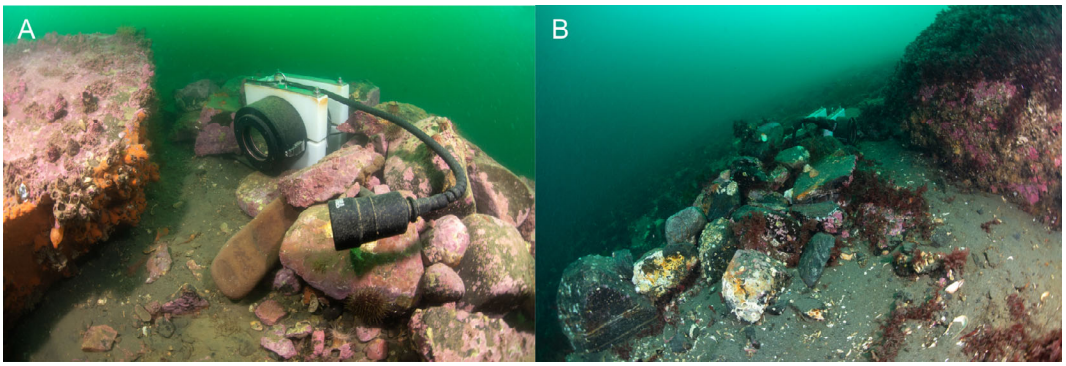

Fig. 5. Comparison of the camera setups: (**A**) camera 3 at Spitsbergen and (**B**) camera 4 in Tromso.

the GLCM can provide redundant information on the texture (Hall-Beyer 2017*b*), it is likely that other features extracted from the GLCM such as the energy or the correlation would provide similar results. GLCM dissimilarity has been used before in an underwater case study from a mobile device (Romero-Ramirez et al. 2016), the novelty presented here relies on its use with underwater static cameras for benthic surveys.

It is to be noted that for a similar period of acquisition, camera 4 had 10 times more invalid images than camera 3. The reason for that can be explained by the layout of the camera in relation with the organisms being monitored (Fig. 5). Camera 3 (Fig. 5A) was set up to record epifaunal organisms (mostly barnacles) located on the overhang and vertical side of the small boulder on a relatively flat seabed, while camera 4 (Fig. 5B) was set up to capture barnacles located directly on the seabed right under the large boulder. This, which a priori seems like an insignificant difference, had a meaningful effect on the acquired data. In the literature there are instances in which epifaunal communities can differ depending on the surface orientation (horizontal vs. vertical; Zintzen et al. 2006; Balazy et al. 2019) as an effect of sedimentation rate, which is very important for filter feeders. Horizontal location means not only a higher possibility of being covered by sediments but also a higher chance of trespassing mobile fauna such as sea stars, brittle stars, hermit crabs, and so on, covering fully or partially either the objects being photographed or the capture system. Furthermore, at the location of camera 4, the slope of the sea floor was much steeper (*see* Fig. 5B). In such an environmental setting, any underwater installation protruding above the seabed acts like a trap/anchor for the detached marine algae and other debris coming from above (Fig. 4C,E,F). Such sites prone to the accumulation of particles of different origin should be avoided whenever possible.

Regardless of the location, artificial objects submerged on the seabed can act as artificial reefs in microscale attracting large numbers of organisms seeking for shelter or food (Balazy et al. 2019). In our case study, animals investigating new items on the seabed are largely responsible for disturbing the view and producing "invalid" images. In addition, artificial light coming from the flash lamp can attract some species, particularly during the typically completely dark conditions of the polar night. This has to be taken into account when securing the camera set-up and light arm at the site. Finally, any irregularities of the camera set-up, even small unevenness of its surface, can be responsible for invalid images. This was the case when sea urchins entered the camera viewfinder depression and stayed moving around constantly for hours (Figs. 1C, 2C).

In conclusion, in order to accelerate automation of subsequent analysis and reduce the computational resources needed, we propose a method based on the dissimilarity of the GLCM to automatically classify images into usable or not usable. In our case study, depending on the data set this method eliminated between 8% and 22% of the images.

Data availability statement

The images used for this study can be requested to Dr. P. Balazy.

References

Aborisade, J. A., J. A. Ojo, A. O. Amole, and A. O. Durodola. 2014. Comparative analysis of textural features derived from GLCM for ultrasound liver image classification. Int. J. Comput. Trends Technol. **11(6)**: 239–244. doi:10.14445/22312803/IJCTT-V11P151.

Aggarwal, A. K. 2022. Learning texture features from GLCM for classification of brain tumor MRI images using random Forest classifier. WSEAS Trans. Signal Process. **18**: 60–63. doi:10.37394/232014.2022.18.8

Balazy, P., P. Kuklinski, and J. Berge. 2018. Diver deployed autonomous time-lapse camera systems for ecological studies. J. Mar. Eng. Technol. **17**: 137–142. doi:10.1080/20464177.2017.1357164

Balazy, P., U. Copeland, and A. Sokołowski. 2019. Shipwrecks and underwater objects of the southern Baltic–Hard substrata islands in the brackish, soft bottom marine environment. Estuar. Coast. Shelf Sci. **225**: 106240. doi:10.1016/j.ecss.2019.05.022

Balazy, P., M. J. Anderson, M. Chelchowski, M. Włodarska-Kowalczuk, P. Kuklinski, and J. Berge. 2021. Shallow-water scavengers of polar night and day—An Arctic time-lapse photography study. Front. Mar. Sci. **8**: 1–10. doi:10.3389/fmars.2021.656772

Barnes, C. R., M. M. R. Best, B. D. Bornhold, S. K. Juniper, B. Pirenne, and P. Phibbs. 2007. The NEPTUNE project—A cabled ocean observatory in the NE Pacific: Overview, challenges and scientific objectives for the installation and operation of Stage I in Canadian waters, p. 308–313. *In* 2007 Symposium on Underwater Technology and Workshop on Scientific Use of Submarine Cables and Related Technologies. IEEE.

Barnes, C. R., M. M. R. Best, F. R. Johnson, L. Pautet, and B. Pirenne. 2011. Challenges, benefits and opportunities in operating cabled ocean observatories: Perspectives from NEPTUNE Canada, p. 1–7. *In* 2011 IEEE Symposium on Underwater Technology and Workshop on Scientific Use of Submarine Cables and Related Technologies. IEEE.

Baschek, B., and others. 2017. The Coastal Observing System for Northern and Arctic Seas (COSYNA). Ocean Sci. **13**: 379–410. doi:10.5194/os-13-379-2017

Bax, N. J., and others. 2019. A response to scientific and societal needs for marine biological observations. Front. Mar. Sci. **6**: 1–22. doi:10.3389/fmars.2019.00395

Bernard, G., A. Grémare, O. Maire, P. Lecroart, F. J. R. Meysman, A. Ciutat, B. Deflandre, and J. C. Duchêne. 2012. Experimental assessment of particle mixing fingerprints in the deposit-feeding bivalve *Abra alba* (Wood). J. Mar. Res. **70**: 689–718.

Bernard, G., J. C. Duchêne, A. Romero-Ramirez, P. Lecroart, O. Maire, A. Ciutat, B. Deflandre, and A. Grémare. 2016. Experimental assessment of the effects of temperature and food availability on particle mixing by the bivalve *Abra alba* using new image analysis techniques. PLoS One **11**: e0154270. doi:10.1371/journal.pone.0154270

Bett, B. J. 2003. Time-lapse photography in the deep sea. Underwater Technol. **25**: 121–127.

Bett, B. J., and A. L. Rice. 1993. The feeding behaviour of an abyssal echiuran revealed by in situ time-lapse photography. Deep Sea Res. Part I Oceanogr. Res. **40**: 1767–1779. doi:10.1016/0967-0637(93)90031-W

Bilodeau, S. M., A. W. H. Schwartz, B. Xu, V. P. Pauca, and M. R. Silman. 2022. A low-cost, long-term underwater camera trap network coupled with deep residual learning image analysis. PLoS One **17**: e0263377. doi:10.1371/journal.pone.0263377

Chatterjee, S., D. Dey, and S. Munshi. 2022. Chapter 3—Extraction of effective hand crafted features from dermoscopic images, p. 53–94. *In* S. Chatterjee, D. Dey, and S. Munshi [eds.], Recent trends in computer-aided diagnostic systems for skin diseases. Academic Press.

Chauvet, P., A. Metaxas, A. E. Hay, and M. Matabos. 2018. Annual and seasonal dynamics of deep-sea megafaunal epibenthic communities in Barkley Canyon (British Columbia, Canada): A response to climatology, surface productivity and benthic boundary layer variation. Prog. Oceanogr. **169**: 89–105. doi:10.1016/j.pocean.2018.04.002

Chauvet, P., A. Metaxas, and M. Matabos. 2019. Interannual variation in the population dynamics of juveniles of the deep-sea crab *Chionoecetes tanneri*. Front. Mar. Sci. **6**: 1–15. doi:10.3389/fmars.2019.00050

Coburn, C. A., and A. C. B. Roberts. 2004. A multiscale texture analysis procedure for improved forest stand classification. Int. J. Remote Sens. **25**: 4287–4308. doi:10.1080/01431160420000192367

Cuvelier, D., F. de Busserolles, R. Lavaud, E. Floc'h, M. C. Fabri, P. M. Sarradin, and J. Sarrazin. 2012. Biological data extraction from imagery—How far can we go? A case study from the Mid-Atlantic Ridge. Mar. Environ. Res. **82**: 15–27. doi:10.1016/j.marenvres.2012.09.001

Duffy, G. A., L. Lundsten, L. A. Kuhnz, and C. K. Paull. 2014. A comparison of megafaunal communities in five submarine canyons off Southern California, USA. Deep-Sea Res. II Top. Stud. Oceanogr. **104**: 259–266. doi:10.1016/j.dsr2.2013.06.002

Eleftheriou, A. 2013. Methods for the study of marine benthos. Wiley-Blackwell.

Estes, M., and others. 2021. Enhanced monitoring of life in the sea is a critical component of conservation management and sustainable economic growth. Mar. Policy **132**: 104699. doi:10.1016/j.marpol.2021.104699

Ferro, C. J. S., and T. A. Warner. 2002. Scale and texture in digital LMAGE classification. Photogramm. Eng. Remote Sens..

Gauci, A., A. Deidun, J. Abela, E. Cachia, and S. Dimech. 2020. Automatic benthic habitat mapping using inexpensive underwater drones, p. 2213–2216. *In* IGARSS 2020–2020 IEEE International Geoscience and Remote Sensing Symposium. IEEE.

Hall-Beyer, M. 2017*a*. GLCM texture: A tutorial v. 3.0.

Hall-Beyer, M. 2017*b*. Practical guidelines for choosing GLCM textures to use in landscape classification tasks over a range of moderate spatial scales. Int. J. Remote Sens. **38**: 1312–1338. doi:10.1080/01431161.2016.1278314

Haralick, R. M. 1979. Statistical and structural approaches to texture. Proc. IEEE. **67**: 786–804.

Haralick, R. M., K. Shanmugam, and I. Dinstein. 1973. Textural features for image classification. IEEE Trans. Syst. Man. Cybern. **SMC-3**: 610–621. doi:10.1109/TSMC.1973.4309314

Jac, C., N. Desroy, J.-C. Duchêne, A. Foveau, C. Labrune, L. Lescure, and S. Vaz. 2021. Assessing the impact of trawling on benthic megafauna: Comparative study of video surveys vs. scientific trawling. ICES J. Mar. Sci. **78**: 1636–1649. doi:10.1093/icesjms/fsab033

Katija, K., E. Orenstein, B. Schlining, and others. 2022. FathomNet: A global image database for enabling artificial intelligence in the ocean. Sci Rep **12**. doi:10.1038/s41598-022-19939-2

Kaufmann, R. S., and K. L. Smith Jr. 1997. Activity patterns of mobile epibenthic megafauna at an abyssal site in the eastern North Pacific: Results from a 17-month time-lapse photographic study. Deep Sea Res. Part I Oceanogr. Res. Pap. **44**: 559–579.

Lampitt, R. S. 1990. Directly measured rapid growth of a deep-sea barnacle. Nature **345**: 805–807. doi:10.1038/345805a0

Maire, O., J. C. Duchêne, R. Rosenberg, J. B. de Mendonça, and A. Grémare. 2006. Effects of food availability on sediment reworking in *Abra ovata* and *A. nitida*. Mar. Ecol. Prog. Ser. **319**: 135–153. doi:10.3354/meps319135

Maire, O., J.-M. Amouroux, J.-C. Duchêne, and A. Grémare. 2007*a*. Relationship between filtration activity and food availability in the Mediterranean mussel *Mytilus galloprovincialis*. Mar. Biol. **152**: 1293–1307. doi:10.1007/s00227-007-0778-x

Maire, O., J. C. Duchêne, A. Grémare, V. S. Malyuga, and F. J. R. Meysman. 2007*b*. A comparison of sediment reworking rates by the surface deposit-feeding bivalve *Abra ovata* during summertime and wintertime, with a comparison between two models of sediment reworking. J. Exp. Mar. Biol. Ecol. **343**: 21–36. doi:10.1016/j.jembe.2006.10.052

Mallet, D., and D. Pelletier. 2014. Underwater video techniques for observing coastal marine biodiversity: A review of sixty years of publications (1952–2012). Fish. Res. **154**: 44–62. doi:10.1016/j.fishres.2014.01.019

Matabos, M., J. Aguzzi, K. Robert, C. Costa, P. Menesatti, J. B. Company, and S. K. Juniper. 2011. Multi-parametric study of behavioural modulation in demersal decapods at the VENUS cabled observatory in Saanich Inlet, British Columbia, Canada. J. Exp. Mar. Biol. Ecol. **401**: 89–96. doi:10.1016/j.jembe.2011.02.041

Matabos, M., N. Piechaud, F. de Montigny, P.-M. Sarradin, and J. Sarrazin. 2015. The VENUS cabled observatory as a method to observe fish behaviour and species assemblages in a hypoxic fjord, Saanich Inlet (British Columbia, Canada). Can. J. Fish. Aquat. Sci. **72**: 24–36. doi:10.1139/cjfas-2013-0611

Pizarro, O., and others. 2013. Benthic monitoring with robotic platforms—The experience of Australia, p. 1–10. *In* 2013 IEEE International Underwater Technology Symposium (UT). IEEE.

Romero-Ramirez, A., A. Grémare, G. Bernard, L. Pascal, O. Maire, and J. C. Duchêne. 2016. Development and validation of a video analysis software for marine benthic applications. J. Mar. Syst. **162**: 4–17. doi:10.1016/j.jmarsys.2016.03.003

Schories, D., M. J. Díaz Aguirre, I. Garrido, T. Heran, J. Holtheuer, J. Kappes, G. Kohlberg, and G. Niedzwiedz. 2020. Analysis of time-lapse images as a tool to study movement in situ in four species of sea urchins and one limpet from North Patagonia and the South Shetland Islands. Antarctic Georef. Biodivers. **30**: 117–136.

She, J., and others. 2019. An integrated approach to coastal and biological observations. Front. Mar. Sci. **6**: 1-6. doi:10.3389/fmars.2019.00314

Smith, C. J., and H. Rumohr. 2013. Imaging techniques, p. 97–124. *In* Methods for the study of marine benthos. John Wiley & Sons, Ltd.

Smith, K. L., Jr., R. S. Kaufmann, and W. W. Wakefieldt. 1993 Mobile megafaunal activity monitored with a time-lapse camera in the abyssal North Pacific. Deep Sea Research Part I: Oceanographic Research Papers, **40**(11), 2307–2324. https://doi.org/10.1016/0967-0637(93)90106-D

Solan, M., B. D. Wigham, I. R. Hudson, R. Kennedy, C. H. Coulon, K. Norling, H. C. Nilsson, and R. Rosenberg. 2004. In situ quantification of bioturbation using time-lapse fluorescent sediment profile imaging (f-SPI), luminophore tracers and model simulation. Mar. Ecol. Prog. Ser. **271**: 1–12. doi:10.3354/meps271001

Soltwedel, T., and others. 2005. HAUSGARTEN: Multidisciplinary investigations at a Deep-Sea, Long-Term Observatory in the Arctic Ocean. Oceanography **18**: 46–61. doi:10.5670/oceanog.2005.24

Spencer, M. L., A. W. Stoner, C. H. Ryer, and J. E. Munk. 2005. A towed camera sled for estimating abundance of juvenile flatfishes and habitat characteristics: Comparison with beam trawls and divers. Estuar. Coast. Shelf Sci. **64**: 497–503. doi:10.1016/j.ecss.2005.03.012

Vardaro, M. F., H. A. Ruhl, and K. L. Smith. 2009. Climate variation, carbon flux, and bioturbation in the abyssal North Pacific. Limnol. Oceanogr. **54**: 2081–2088.

Williams, S. B., and others. 2012. Monitoring of benthic reference sites: Using an autonomous underwater vehicle. IEEE Robot. Autom. Mag. **19**: 73–84.

Zintzen, V., C. Massin, A. Norro, and J. Mallefet. 2006. Epifaunal inventory of two shipwrecks from the Belgian Continental Shelf. Hydrobiologia **555**: 207–219.

Acknowledgment

This study received funding from the National Science Centre, Poland, project no. 2018/29/B/NZ8/02340.

Submitted 18 August 2022
Revised 25 January 2023
Accepted 29 January 2023

Associate editor: Scott Ensign